Citation: **Hirt, C**. and Kuhn, M. (2014), Band-limited topographic mass distribution generates full-spectrum gravity field – gravity forward modelling in the spectral and spatial domains revisited, Journal of Geophysical Research - Solid Earth, 119(4), 3646–3661, doi: 10.1002/2013JB010900.

Band-limited topographic mass distribution generates full-spectrum gravity field – gravity forward modelling in the spectral and spatial domains revisited

Christian Hirt

Western Australian Centre for Geodesy & The Institute for Geoscience Research,
Curtin University, GPO Box U1987, Perth, WA 6845, Australia
Email: c.hirt@curtin.edu.au

Currently at:
Institute for Astronomical and Physical Geodesy & Institute for Advanced Study
Technische Universität München, Germany

Michael Kuhn

Western Australian Centre for Geodesy &The Institute for Geoscience Research,
Curtin University, GPO Box U1987, Perth, WA 6845, Australia
Email: m.kuhn@curtin.edu.au

Key points

- Band-limited topographic mass model generates a full-spectrum gravity field
- p-th power of topography expanded to n contributes to degree p × n to potential
- Spatial and spectral gravity forward-modelling techniques agree at 10^{-5} level

Abstract

Most studies on gravity forward modelling in the spectral domain truncate the gravitational potential spectra at a resolution commensurate with the input topographic mass model. This implicitly assumes spectral consistency between topography and implied topographic potential. Here we demonstrate that a band-limited topographic mass distribution generates gravity signals with spectral energy at spatial scales far beyond the input topography's resolution. The spectral energy at scales shorter than the resolution of the input topography is associated with the contributions made by higher-order integer powers of the topography to the topographic potential. The p-th integer power of a topography expanded to spherical harmonic degree n is found to make contributions to the topographic potential up to harmonic degree p times n. New numerical comparisons between Newton's integral evaluated in the spatial and spectral domain

show that this previously little addressed truncation effect reaches amplitudes of several mGal for topography-implied gravity signals. Modelling the short-scale gravity signal in the spectral domain improves the agreement between spatial and spectral domain techniques to the microGal-level, or below 10^{-5} in terms of relative errors. Our findings have important implications for the use of gravity forward modelling in geophysics and geodesy: The topographic potential in spherical harmonics must be calculated to a much higher harmonic degree than resolved by the input topography if consistency between topography and implied potential is sought. With the improved understanding of the spectral modelling technique in this paper, theories and computer implementations for both techniques can now be significantly better mutually validated.

Key words: Gravity, topography, gravity forward modelling, spatial modelling, spectral modelling

1 Introduction

Gravity forward modelling denotes the computation of the gravitational signal (e.g., in terms of gravitational potential, gravity disturbances or gravity gradients) induced by a mass-density distribution, as given, e.g., through topographic mass models. Techniques for gravity forward modelling are routinely applied in potential field geophysics, e.g., to aid the interpretation of observed gravity [*Jakoby and Smilde,* 2009] and in physical geodesy, e.g., in the context of geoid modelling [*Tziavos and Sideris,* 2013]. Common to all gravity forward modelling techniques is the evaluation of the well-known Newton's integral, which can be done both in the spatial domain and spectral domain [*Kuhn and Seitz,* 2005; *Wild-Pfeiffer and Heck,* 2007].

- Spatial domain forward modelling [e.g., *Forsberg,* 1984; *Nagy et al.* 2000; *Kuhn et al.* 2009; *Tsoulis et al.* 2009; *Hirt et al.,* 2010; *Grombein et al.,* 2013; *d'Urso,* 2014] directly evaluates Newton's integral. This is commonly done by decomposing the topographic mass model into elementary bodies (e.g., prisms, tesseroids, polyhedra) along with numerical/analytical integration to obtain the gravitational potential implied by the masses. This technique is also known as Newtonian integration.

- Spectral domain forward modelling [e.g., *Sünkel,* 1985; *Rummel et al.* 1988; *Tenzer*, 2005; *Wieczorek,* 2007; *Novák,* 2010; *Hirt and Kuhn,* 2012] evaluates Newton's integral through transformation into the spectral domain. This commonly utilizes spherical-harmonic series expansions for conversion of spherical harmonic topography models to the implied gravitational potential. Formulated as a three-step procedure, in spectral forward modelling (i) the topographic surface (i.e., the topographic heights sampled on a geographical grid) and its integer powers are expanded into spherical harmonic series. The resulting coefficients are (ii) directly used to yield the topographic potential in spherical harmonics (as a series expansion of the integer powers of the topography), and (iii) gravity effects are obtained from the topographic potential coefficients in the spatial domain through spherical harmonic synthesis.

Many previous studies concerned with spectral domain forward modelling use a spherical harmonic topography model to some fixed spectral resolution (as specified through the maximum harmonic degree of the series expansion, e.g., 360) for the calculation of implied gravitational potential with identical resolution. As such, spectral consistency (i.e., identical spectral band widths) of the topography and generated gravitational potential is implicitly assumed. Examples of such works are *Sünkel* [1985]; *Rummel et al.* [1988]; *Rapp* [1989]; *Rapp and Pavlis* [1990]; *Pavlis and Rapp* [1990]; *Tsoulis* [2001]; *Kuhn and Featherstone* [2003]; *Wild-Pfeiffer and Heck* [2007]; *Wieczorek* [2007]; *Mahkloof* [2007]; *Novák* [2010]; *Balmino et al*. [2012]; *Hirt et al.* [2012]; *Hirt and Kuhn* [2012]; *Tenzer et al.* [2012]; *Bagherbandi and Sjöberg*, [2012]; *Novák and Tenzer* [2013]; *Gruber et al.,* [2014], among others. However, as will be shown in this paper, this mostly unwritten assumption does not hold, see also *Heck and Seitz* [1991], and *Papp and Wang* [1996].

As the main topic of the present study we demonstrate that a band-limited spherical harmonic topography generates (in good approximation) a full-banded gravitational potential. We show that the generated gravitational signal features additional high-frequency spectral energy beyond and far beyond the initial band limitation of the input (source) topography. This effect, which causes "spectral inconsistency" between topography and gravitational signal, is fairly straightforward to model (Section 2), but mostly neglected in the literature. We will show this effect to be responsible for spurious discrepancies in numerical comparisons among gravitational signals from spectral and space domain techniques (Section 3).

In previous studies concerned with comparisons among gravitational effects from the two techniques, notable discrepancies were encountered or reported. In terms of *relative errors* (defined here as the ratio between the maximum discrepancy between spatial and spectral forward modelling and the maximum gravitational signal over some test area)

- *Kuhn and Seitz* [2005] found relative errors at the level of ~3 % for the gravitational potential, for expansions to harmonic degree 1440,
- *Wild-Pfeiffer and Heck* [2007] yielded relative errors of ~4.5 % for gravity gradients over a global test area (maximum signals of ~6.7 Eötvos (1 Eötvös = 10^{-9} s^{-2}) versus a maximum discrepancy of ~0.3 Eötvos),
- *Wang et al.* [2010] encountered relative errors at the level of ~10% or up to ~60 mGal(1 mGal = 10^{-5} ms^{-2}) discrepancies for gravity disturbances over various mountainous test areas (e.g., Himalayas, Rocky Mountains, Andes) for expansions to harmonic degree 2700,
- *Balmino et al.* [2012] published discrepancies at the level of ~10 % (or up to ~48 mGal) for gravity disturbances over their test area 'Marocco', and
- *Novák and Tenzer* [2013] found relative errors of ~0.8% for gravity gradients at satellite altitude over a regional test profile crossing the Andes (maximum discrepancy of 0.5 × 10^{-2} Eötvös versus signal of 5.8 Eötvös),

please also see discussion in Section 4. The five aforementioned studies have in common that they do not investigate the spectral inconsistency between topography and implied gravity as a key candidate for the differences encountered. While the spatial domain technique (Newtonian integration) implicitly takes into account the additional high-frequency spectral constituents beyond the band width of the input topography, explicit consideration is required in the spectral domain for improved mutual consistency of gravity effects from the two forward modelling techniques.

From our literature review, the spectral inconsistency among topography and gravity is only little discussed in the context of gravity forward modelling, though the mechanisms affecting the spectral characteristics are by no means unknown. *Papp and Wang* [1996] modelled the gravitational potential in spherical harmonics and noticed truncation effects in comparisons with Newtonian integration. They made the important statement that "[…] *the spectral characteristics of the spherical harmonics in forward local gravity modelling are different from that of the results obtained from rectangular prism integration.*" [*Papp and Wang*, 1996, p63]. *Heck and Seitz* [1991] investigated nonlinear effects in the geodetic boundary value problem, showing that the multiplication of two series expansions to represent second-order effects increases the maximum harmonic degree by a factor of 2. In the context of the frequently used geodetic reference system GRS80 (*Moritz,* [2000]), another analogy is found [*Claessens,* 2013, pers. comm.]. A rotating mass-ellipsoid (as "example" for a most simple spherical harmonic topography) generates a gravitational field with notable spectral energy at even multiples of degree 2.

The first and main aim of the present study is the introduction of a novel contribution scheme for spectral domain forward modelling that relies on spherical harmonic topographic mass models of some given resolution as input data. Our scheme provides the spectral constituents of the implied gravity signal at all spatial scales – to and beyond the input topography's resolution. As second aim of the study, we use the contribution scheme in new comparisons between spectral and spatial forward modelling techniques to demonstrate that high-frequency gravity signals (beyond the input topography's resolution) are naturally 'delivered' by space domain techniques, while the spectral technique requires explicit modelling. Our new contribution scheme is suitable to do this. As further aims, we demonstrate the practical relevance of the higher-order integer power contributions of the topography to the implied potential, the importance of the computation point height in both techniques, and the convergence of series expansions used for field continuation in the spectral domain.

The paper is organized as follows. Section 2 sets the mathematical framework for spatial and spectral domain forward modelling, exemplified here for gravity disturbances as radial derivatives of the gravitational potential. Section 3 then presents a numerical case study which (i) analyses the spectra of the topography-implied gravitational potential and (ii) compares gravity from spatial and spectral domain forward modelling. The case study demonstrates that explicit modelling of the high-frequency spectrum in the spectral domain significantly improves

151 the agreement with spatial forward modelling. Section 4 discusses the results, also in the context
152 of the literature, and Section 5 draws conclusions for some present and future gravity forward
153 modelling applications.

154 **2 Theory**

155 We start by introducing H_{nm} as a short-hand for the fully-normalized spherical harmonic
156 coefficients (SHC) $(\overline{HC}, \overline{HS})_{nm}$ of a topography model, whereby n denotes the harmonic degree,
157 and m the harmonic order. The coefficients H_{nm} are expanded into the spherical harmonic series

158 $$H(\varphi,\lambda) = \sum_{n=0}^{n_{\max}} \sum_{m=0}^{n} (\overline{HC}_{nm} \cos m\lambda + \overline{HS}_{nm} \sin m\lambda) \overline{P}_{nm}(\sin\varphi) \qquad (1)$$

159 to maximum degree $n_{\max}$ in order to describe the topographic height $H(\varphi,\lambda)$ at geocentric
160 latitude φ and longitude λ. The term $\overline{P}_{nm}(\sin\varphi)$ denotes the fully-normalized associated
161 Legendre function of degree n and order m. Topographic heights H are laterally variable and
162 provide the height of the topographic surface with respect to some height reference surface, e.g.,
163 mean sea level. The harmonic coefficients H_{nm} are assumed to be readily available from a
164 spherical harmonic analysis of some global topography model (cf. Section 3).

165 The spherical harmonic topography model expanded to maximum degree $n_{\max}$ is used as input
166 (i.e., source model that generates the topographic gravity field) both for the spatial domain
167 (Section 2.1) and spectral domain forward modelling (Section 2.2) along with some constant
168 mass-density value ρ (e.g., of standard rock). This is done in order to use identical topographic
169 mass models as "source of the gravity field" in both techniques. We acknowledge that laterally-
170 varying mass-density values could be used as a refinement [e.g., *Kuhn and Featherstone* 2003;
171 *Eshagh,* 2009], but this is not necessary for the topic of our study.
172
173 For reasons of simplification, we consistently use the spherical approximation for forward
174 modelling with both techniques. In the spherical approximation, the topographic height H is
175 „mapped" onto the surface of a reference sphere with some constant radius R (see, e.g., *Balmino*
176 *et al.,* [2012]). The spherical approximation is chosen here over the more advanced ellipsoidal
177 approximation [*Claessens and Hirt,* 2013; *Wang and Yang,* 2013] which uses a reference
178 ellipsoid instead of a reference sphere. The spherical approximation level chosen is completely
179 suitable to compare the spectral characteristics of the topography with the implied topographic
180 potential. The spherical approximation is also used for reasons of consistency with the vast
181 majority of previous works on forward-modelling (see references in the introduction).

182

2.1 Spatial domain forward modelling

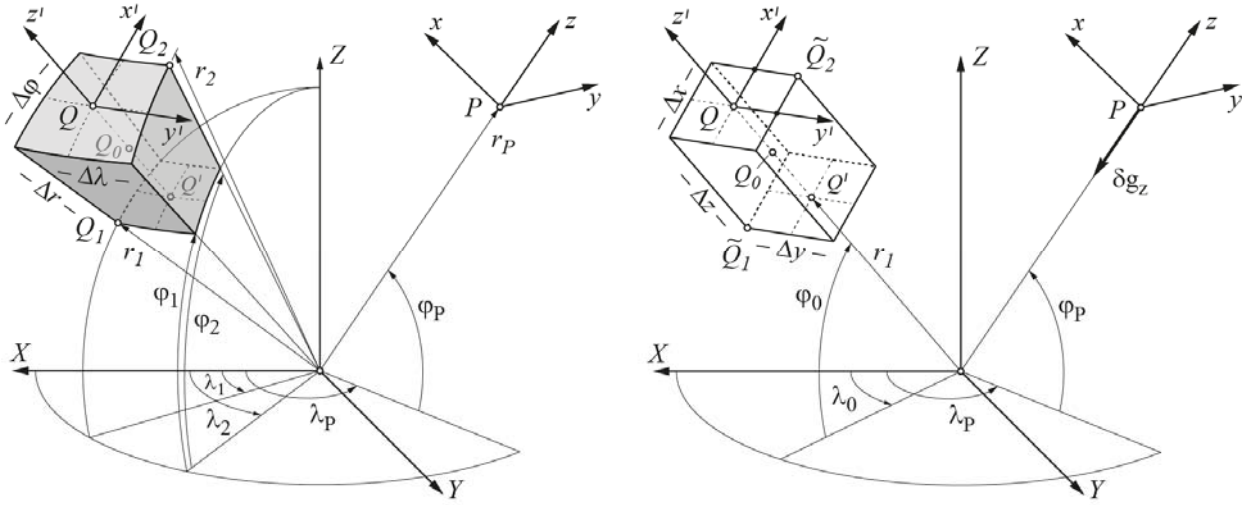

Figure 1. Geometry of a tesseroid (left) replaced by a rectangular prim with first-order mass equivalence and identical vertical extension (right). Note, while the intersection points Q and Q' of the centre line with the tesseroid's top and bottom surfaces are identical with that of the prism, the corner points are not (e.g. $Q_1 \neq \widetilde{Q}_1$ and $Q_2 \neq \widetilde{Q}_2$).

Spatial domain forward modelling of the global topographic masses is based on *discretised* Newtonian integration following the concepts applied in, e.g., *Kuhn* [2000], [2003] and *Kuhn et al.* [2009]. In this approach the mass distribution considered is discretised by a set of regularly shaped mass elements (e.g. point mass, prism or tesseroid) and the gravitational signal is obtained through superposition of the individual effects from each mass element. This principle is exemplified by Eq. (2) through Newton's integral for the gravitational potential δV generated by the mass distribution M replaced by the sum over the gravitational potentials δV_n generated by N_{elem} mass elements m_n ($n = 1, \ldots, N_{elem}$).

$$\delta V = G \iiint_M \frac{dm}{l} \approx \sum_{n=1}^{N_{elem}} G \iiint_{m_n} \frac{dm_n}{l_n} = \sum_{n=1}^{N_{elem}} \delta V_n \qquad (2)$$

In Eq. (2), G is the universal gravitational constant, and dm and dm_n denote infinitesimally small mass elements describing M and m_n, respectively. The Euclidian distances l and l_n are defined between the computation point P and the running integration points within M and m_n, respectively. We calculate the gravitational attraction δg_z (radial derivative of the potential, also known as gravity disturbance) along the vertical at P (i.e., in opposite direction to the surface normal on a reference sphere) via

$$\delta\vec{g} = \left(\delta g_x, \delta g_y, \delta g_z\right)^T = \mathrm{grad}(\delta V) \approx \sum_{n=1}^{N} \mathrm{grad}(\delta V_n) \tag{3}$$

Where grad denotes the gradient and $\delta g_x, \delta g_y, \delta g_z$ are the vector components of $\delta\vec{g}$ given with respect to a topocentric coordinate system *x,y,z* at *P* (cf. Fig. 1). The coordinate axes of the topocentric coordinate system are orientated so that the *x*-axis points towards geodetic north, the *y*-axis towards geodetic east and the *z*-axis towards the zenith (or radial direction).

The approximation errors introduced by Eqs. (2) and (3) depend on how well the elements m_n approximate the original mass distribution *M*. The use of rectangular prisms is approximate because the vertical faces of adjoining prisms are not parallel (they intersect or exhibit wedge-like gaps). An upper limit of the magnitude of this effect on the order of 2 μGal (= 2×10^{-8} ms^{-2}) in this study is obtained from the numerical comparisons between the space and spectral domain techniques (Section 3.4). In future application of the space domain technique, polyhedra [e.g., *Benedek*, 2004; *d'Urso*, 2014] can be a viable alternative to prisms because they avoid the prism approximation. In order to reduce approximation errors caused by mass elements located in the vicinity of the computation point we divide the gravitational attraction according to

$$\delta\vec{g} = \delta\vec{g}^{SH} + \delta\vec{g}^{RM} \tag{4}$$

where $\delta\vec{g}^{SH}$ is the gravitational attraction of a shell (or more generally a layer) of constant thickness and $\delta\vec{g}^{RM}$ is the gravitational attraction of all masses residual to the shell. The shell is selected such that no residual masses are present at the location of the computation point. In this study we model the topographic masses (including bathymetry and ice sheets, cf. Sect. 3.2) in spherical approximation, thus $\delta\vec{g}^{SH}$ corresponds to the gravitational attraction of a spherical shell (often termed Bouguer shell) and $\delta\vec{g}^{RM}$ corresponds to the spherical terrain correction [e.g., *Kuhn et al.* 2009].

For the practical evaluation of $\delta\vec{g}$, in this study, we replace the topographic masses by a series of tesseroids in spherical approximation, which are further approximated by rectangular prisms with first-order mass equivalence and identical vertical extension. The methodology and corresponding formulae are provided by e.g. *Anderson* [1976]; *Grüninger* [1990]; *Kuhn* [2000] and *Heck and Seitz* [2007] and will be briefly outlined here.

Tesseroids in spherical approximation are spherical mass elements bounded by surfaces of constant geocentric latitude (φ_1, φ_2), longitude (λ_1, λ_2), and geocentric radii ($r_1 = R + H_1, r_2 = R + H_2$) and can be considered as the *natural* mass element when using heights *H* (here from Eq. 1) given on a regular geocentric latitude-longitude grid (Fig. 1). The

geometrical centre $Q_0(\varphi_0, \lambda_0, r_0)$ and dimensions $(\Delta\varphi, \Delta\lambda, \Delta r)$ of the tesseroid are given by (cf. Fig. 1)

$$\varphi_0 = (\varphi_1 + \varphi_2)/2\,; \qquad \Delta\varphi = \varphi_2 - \varphi_1 \tag{5}$$
$$\lambda_0 = (\lambda_1 + \lambda_2)/2\,; \qquad \Delta\lambda = \lambda_2 - \lambda_1$$
$$r_0 = (r_1 + r_2)/2\,; \qquad \Delta r = r_2 - r_1$$

As the integral over m_n in Eq. (2) cannot be exactly solved for a tesseroid [cf. *Heck and Seitz* 2007] we approximate the tesseroid by a rectangular prism centred at the same location Q_0 with its edges being parallel to the axes x', y', z' of a topocentric coordinate system located at the centre of the tesseroid's top surface $Q(\lambda_0, \varphi_0, r_2)$ which coincides with the centre of the prism's top surface (cf. Fig. 1). For first-order mass equivalence and identical heights the dimension of the prism is given by [e.g., *Anderson,* 1976; *Grüninger,* 1990; *Heck and Seitz,* 2007]:

$$\Delta x = r_0 \Delta\varphi\,; \qquad \Delta y = r_0 \cos\varphi_0 \Delta\lambda\,; \qquad \Delta z = \Delta r \tag{6}$$

We compute the gravitational attraction of the rectangular prisms based on the well-known analytical formulae as provided by e.g. *Mader* [1951]; *Nagy* [1966]; *Nagy et al.* [2000, 2002] and modified to a numerically more stable expression shown in e.g. *Kuhn* [2000] and *Heck and Seitz* [2007]. Within our numerical studies we only focus on the z-component δg_z (the gravity disturbance) of the vector $\delta\vec{g}$ (cf. Eq. 3) at the location of the computation point P (cf. Fig. 1).

2.2 Spectral domain forward modelling

The technique description is largely based on the work by *Hirt and Kuhn* [2012], but modified here to accommodate for the additional high-frequency spectral constituents beyond the band-width of the input topography.

2.2.1 Topographic potential in the spectral domain

The key ingredient for spectral domain forward modelling are topographic height functions and their integer powers. We define the dimensionless topographic height function (THF) as ratio of the topographic height H and the reference radius R. The THF raised to arbitrary integer power p ($p \in \mathbb{N}$) then reads

$$H^{(p)} = \frac{H^p}{R^p} \tag{7}$$

in the spatial domain. The spectral domain representation of $H^{(p)}$, denoted here with $H^{(p)}_{nm} = (\overline{HC}, \overline{HS})^{(p)}_{nm}$, is obtained through spherical harmonic analyses of the $H^{(p)}$. The $H^{(p)}_{nm}$ of the THF are thus related to their spatial domain counterpart $H^{(p)}(\varphi, \lambda)$ via

$$H^{(p)}(\varphi,\lambda)=\sum_{n=0}^{N_{\max}}\sum_{m=0}^{n}(\overline{HC}_{nm}^{(p)}\cos m\lambda+\overline{HS}_{nm}^{(p)}\sin m\lambda)\bar{P}_{nm}(\sin\varphi) \quad (8)$$

where the maximum harmonic degree $N_{\max}$ is commonly set identical with the maximum degree $n_{\max}$ of the topography model, and thus considered independent of the integer power p, e.g.,

$$N_{\max}=n_{\max}. \quad (9)$$

The vast majority of past works on spectral domain forward modeling relies [implicitly] on Eq. (9), see the list of cited references in the introduction. As novelty of this study, we here extend the spectral forward modeling technique by introducing $N_{\max}$ as a function of the integer power p for the THFs, *e.g.,*

$$N_{\max}=pn_{\max} \quad (10)$$

and therefore

$$H^{(p)}(\varphi,\lambda)=\sum_{n=0}^{pn_{\max}}\sum_{m=0}^{n}(\overline{HC}_{nm}^{(p)}\cos m\lambda+\overline{HS}_{nm}^{(p)}\sin m\lambda)\bar{P}_{nm}(\sin\varphi) \quad . \quad (11)$$

Increasing the maximum harmonic degree $N_{\max}$ from $n_{\max}$ to $pn_{\max}$ requires oversampling of the $H^{(p)}$ by factor p prior to computing the $H_{nm}^{(p)}$ via the spherical harmonic analyses. Compared to the maximum harmonic degree $n_{\max}$ of the topography model, twice the spectral resolution ($2n_{\max}$) is thus taken into account for the squared THF $H_{nm}^{(2)}$, and three times the resolution ($3n_{\max}$) for the cubed THF $H_{nm}^{(3)}$, and so forth.

The topographic gravitational potential (short: topographic potential) coefficients V_{nm} are calculated via a standard series expansion into powers p of the THFs $H_{nm}^{(p)}$ [after *Wieczorek* 2007, *Hirt and Kuhn* 2012]:

$$V_{nm}=\frac{1}{2n+1}\frac{4\pi R^3\rho}{M}\sum_{p=1}^{p\max}\frac{\prod_{i=1}^{p}(n+4-i)}{p!(n+3)}H_{nm}^{(p)} \quad (12)$$

where V_{nm} is the short-hand for the $(\overline{VC},\overline{VS})_{nm}$ SHCs of the topographic potential, $p_{\max}$ is the maximum integer power of the series expansion, and *M* is the mass of the planet. From *Hirt and Kuhn* [2012, Fig. 1 ibid], the higher the resolution of the input topography $n_{\max}$, the more integer powers *p* must be taken into account in Eq. (12) for convergence. The number of terms also

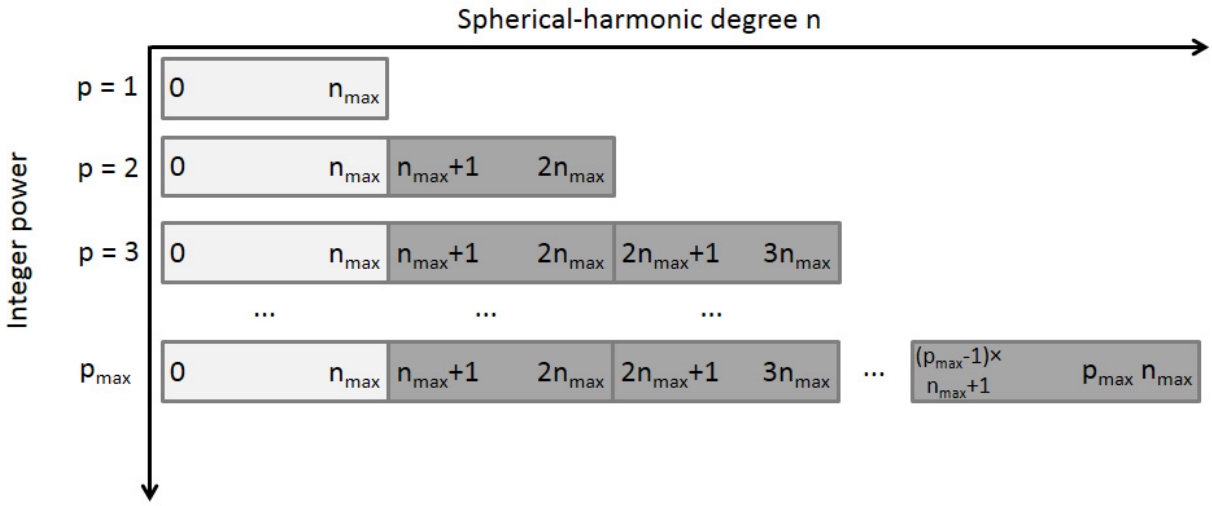

Figure 2. Contribution scheme for spectral domain gravity forward modelling: Contributions of integer powers p of the topography to the topographic potential as a function of the integer power (vertical axis) and the p-th multiple of the input bandwidth (horizontal axis)

increase with the range of the heights relative to the reference radius R, see *Claessens and Hirt* [2013]. For degree-2160 Earth topography mass models, it was shown that $p_{\max} = 8$ yields truncation errors (resulting from dropping terms with $p > 8$) well below the mGal level, cf. *Hirt and Kuhn* [2012]. Another convergence analysis has shown truncation errors below the mGal level for degree 360 models and $p_{\max} = 4$ [*Wieczorek* 2007].

Eq. (12) can easily be evaluated for individual integer powers p, instead of calculating the sum from $p = 1$ to $p_{\max}$. Then, the contribution of the p-th integer power of the topography to the topographic potential is obtained. Eq. (12) can also be evaluated separately for harmonic band $n \in [0 \quad n_{\max}]$ and for p-th multiples thereof: $n \in [(p-1)n_{\max} + 1 \quad pn_{\max}]$. This leads to a new, generalized contribution scheme for spectral domain forward modelling shown in Fig. 2.

The left column (light grey boxes in Fig. 2) shows the contribution of the p-th integer power of the topography limited to $n_{\max}$, these were investigated or calculated e.g., by *Rummel et al.* [1988]; *Tsoulis* [2001]; *Wild-Pfeiffer and Heck* [2007]; *Wieczorek* [2007]; *Mahkloof* [2007]; *Novák* [2010]; *Balmino et al.* [2010]; *Hirt and Kuhn* [2012], among many others.

New are the columns with $n > n_{\max}$ (dark grey boxes in Fig. 2). They reflect the additional high-frequency signals associated with forming powers of the THF. Raising the THF to power $p = 2$ doubles the band-width of the input topography, and power $p = 3$ triples the input band width, leading to the triangular contribution scheme in Fig. 2. This can be generalized to the statement:

The p-th integer power of a topography expanded to spherical harmonic degree n_{max} contributes to the topographic potential up to degree p times n_{max}.

This finding can be easily verified by the frequencies present in the p-th powers of sine or cosine-functions (cf. Fig. 3). For instance, raising the sine function with frequency f_0 to the 2nd power doubles the frequency, e.g. $2f_0$, compared to the sine function. For the 3rd power the maximum frequency present is $3f_0$ and so forth for higher powers (Fig. 3). Raising the sine function to infinite power will result in an infinite sequence of equidistant delta functions of which the Fourier transform is also an infinite series of equidistant delta functions covering infinite multiples of f_0 [e.g., *Bringham,* 1988, p21]. This behaviour is exemplified with a sine function raised to power p= 1000 in Fig. 3.

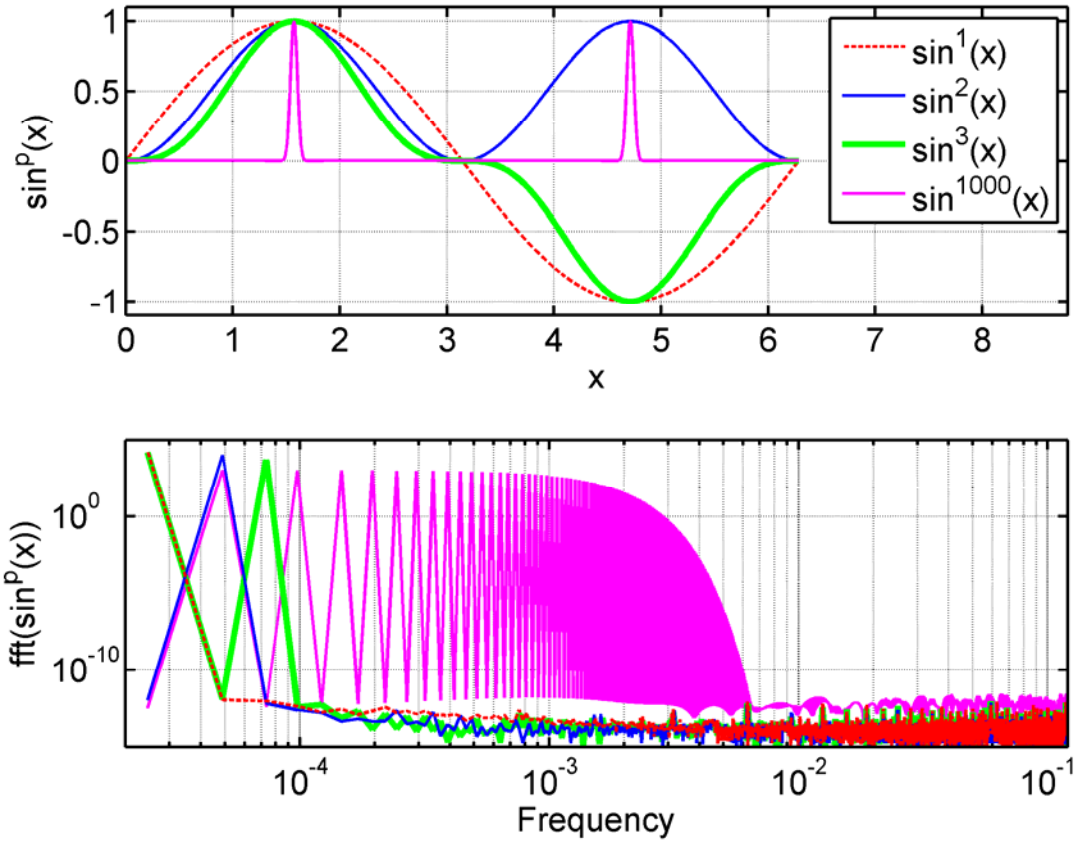

Figure 3. Top: Sine-functions raised to integer powers p = 1,2, 3 and 1000, Bottom: Fourier-spectra (magnitudes) of the powered sine functions. The bottom panel exemplifies the gain in band-width as the power p increases. Variable x in radian, frequencies normalized to interval [0 1].

Applying this analogy to the topography function H expressed through a series of sine and cosine functions (cf. Eq. 1) covering the spectral band to a maximum degree n_{max}, e.g. $n \in [0 \quad n_{max}]$ the

spectral band of the squared function extends to $2n_{\max}$, as noted by *Heck and Seitz* [1991]. Ultimately, raising H to infinite power will result in a function covering the full spectrum even though the original function was band-limited. This behaviour can also be verified by analysing the spectra of the powered THFs (Sect. 3.3), thus confirming the contribution scheme. Further evidence in support of the contribution scheme is gathered by comparisons between gravity from space and spectral domain techniques (Sect. 3.4).

2.2.2 Synthesis of functionals of the potential

The V_{nm} can be used to calculate the topographic potential or various functionals thereof in the spatial domain at the three-dimensional coordinates geocentric latitude φ, longitude λ and geocentric radius r via spherical harmonic synthesis [e.g., *Holmes and Pavlis* 2008; *Hirt* 2012]. Here we evaluate the frequently used gravity disturbance δg (being the radial derivative of the gravitational potential, equivalent to δg_z introduced in Sect. 2.1), defined through [after *Torge* 2001, p 271]:

$$\delta g(\varphi,\lambda,r) = -\frac{\partial V}{\partial r} = \frac{GM}{r^2}\sum_{n=2}^{n\max}(n+1)\left(\frac{R}{r}\right)^n\sum_{m=0}^{n}(\overline{VC}_{nm}\cos m\lambda + \overline{VS}_{nm}\sin m\lambda)\overline{P}_{nm}(\sin\varphi) \quad . \tag{13}$$

As geocentric radius r of the evaluation points, we choose the surface of the topographic mass model, as represented through

$$r = r(\varphi,\lambda) = R + H(\varphi,\lambda) \tag{14}$$

This is done in order to account for the effect of gravity attenuation with height [cf. *Hirt* 2012]. For reasons outlined in *Hirt* [2012], and *Hirt and Kuhn* [2012], evaluation of Eq. (13) in terms of dense grids can be computationally demanding when the radii of evaluation $r(\varphi,\lambda)$ vary along parallels ($\varphi =$ constant), as in Eq. (14). A numerically efficient and precise approximate solution is obtained here via field continuation of gravity disturbances with higher-order gradients of δg [*Hirt and Kuhn,* 2012]

$$\delta g^{k\max}(\varphi,\lambda,r) \approx \sum_{k=0}^{k\max}\frac{1}{k!}\left.\frac{\partial^k\delta g}{\partial r^k}\right|_{r=R+H_{ref}}(H-H_{ref})^k \tag{15}$$

where $k_{\max}$ is the maximum order of the series expansion, H_{ref} is some mean reference height for acceleration of convergence and $\partial^k\delta g/\partial r^k$ is the *k*-th order radial derivative of δg calculated at a constant height $r = R + H_{ref}$ via [*Hirt*, 2012]

$$\frac{\partial^k \delta g}{\partial r^k} = (-1)^k \frac{GM}{r^{k+2}} \sum_{n=2}^{n\max} (n+1) \left\{ \prod_{i=1}^{k} (n+i+1) \right\} \left(\frac{R}{r} \right)^n \times \sum_{m=0}^{n} (\overline{VC}_{nm}^{p\max} \cos m\lambda + \overline{VS}_{nm}^{p\max} \sin m\lambda) \overline{P}_{nm}(\sin\varphi) \quad (16)$$

3 Numerical study

3.1 General

A numerical study is carried out based on the publicly available RET2012 topography model (Sect 3.2) with the goals to analyse the spectra of the THFs (Sect. 3.3.1) and of their contributions to the topographic potential (Sect. 3.3.2) in order to investigate the signal strengths of these contributions for gravity disturbances in the spatial domain. The study then systematically compares gravity disturbances from spatial and spectral domain forward modelling as a function of the p *-th* integer power contributions and maximum harmonic degree $N_{\max} = pn_{\max}$ taken into consideration (Sect. 3.4). A main motivation for the numerical study is the verification of the contribution scheme for spectral domain forward modelling (Fig. 2).

For the spherical harmonic synthesis of the topography H [Eq. (1)], and analyses of the THFs $H_{nm}^{(p)}$ [Eq. (7)] we use the SHTools package (www.shtools.org), and for spherical harmonic synthesis of gravity disturbances and their k -th order radial derivatives [cf. Eq. (16)] a modification of the harmonic_synth software [*Holmes and Pavlis,* 2008]. Both packages deploy the routines by *Holmes and Featherstone* [2002] for the stable computation of the associated Legendre functions $\overline{P}_{nm}(\sin\varphi)$ to degree n =2700. Given that the $\overline{P}_{nm}(\sin\varphi)$ are subject to numerical instabilities which increase for $n > 2700$ [*Holmes and Featherstone*, 2002], we confine all of our numerical tests to

$$N_{\max} = pn_{\max} \le 2700. \quad (17)$$

As a consequence, the band width $[0 \quad n_{\max}]$ of the input topography must be chosen sufficiently narrow to allow for accurate evaluation of the high-frequency p-multiples of $[0 \quad n_{\max}]$. Among many possible band widths, we have chosen the input band $[0 \quad n_{\max} = 360]$ as our example for band-limited topographic mass models. For this band, calculation and analyses of multiples of the input band $[0 \quad n_{\max} = 360]$ up to p = 7 is safely possible. As will be shown, this is sufficient to verify the contribution scheme in Fig. 1.

We acknowledge that algorithms for the stable computation of $\overline{P}_{nm}(\sin\varphi)$ to arbitrary degree have been developed [*Fukushima,*2012a; 2012b], which could be used in a future case study to ultra-high degree, once tested implementations for spherical harmonic analyses become available

(for spherical harmonic synthesis software to ultra-high degree see e.g., *Bucha and Janák* [2013]).

3.2 Data and constants

As model representing the topographic masses, we use the freely-available spherical harmonic data set RET2012 (rock-equivalent topography model) of Curtin University's Earth2012 model suite (URL: http://geodesy.curtin.edu.au/research/models/Earth2012/, file Earth2012.RET2012.SHCto2160.dat). This allows replication of our study. Based on a range of input data sets, RET2012 represents the masses of the visible topography, of the oceans and major inland lakes, and major ice-sheets using a single constant mass-density of ρ = 2670 kg m^{-3}. Rock-equivalent heights of ice and water-masses were derived through mathematical compression into rock equivalent mass layers [e.g., *Rummel et al., 1988*], see *Hirt et al.* [2012] and *Hirt* [2013] for details on the procedures applied to generate the RET2012 SHCs H_{nm}. Though the SHCs of RET2012 are available to degree and order 2160, we use this model only from degree and order 0 to degree and order 360 ($=n_{\max}$). As such, only the RET2012 spectral band of harmonic degrees 0 to 360 defines the input (source) topography in this study.

For our tests of the two forward-modelling techniques, we use exactly the same topographic mass model as input: In the spatial domain technique: heights $H(\varphi,\lambda)$ synthesized from the RET2012SHCs H_{nm} at various resolutions, and in the spectral domain technique the H_{nm} directly as input topography. Also used with identical numerical values in both techniques are the topographic mass density ρ = 2670 kg m^{-3}, reference radius $R = 6{,}378{,}137$ m (semi-major axis of GRS80), [*Moritz,* 2000], the universal gravitational constant G= 6.67384 × 10^{-11} m^3 kg^{-1} s^{-2} [*Mohr et al.* 2012, p 72] and total Earth's mass (including atmosphere) M = 5.9725810 × 10^{24} kg (from the *GM* product of GRS80, *Moritz* [2000]).

3.3 Spectral analyses

3.3.1 Topography

To derive the spectra of the THFs, we (i) synthesized RET2012 heights H in spectral band $[0 \quad n_{\max} = 360]$ in terms of regularly-spaced geocentric latitude-longitude grid of 2 arc-min resolution (5400 × 10800 heights), (ii) normalized this grid with R, (iii) raised the resulting THFs to integer power $p \geq 1$, and (iv) analysed harmonically the powered THFs $H^{(p)}$ with SHTools (algorithm by *Driscoll and Healy* [1994]). This procedure gave us the $H_{nm}^{(p)}$-SHCs to a maximum degree and order $n = m$ = 2700. Note that the THFs assume very small values as the power increases (e.g., p= 5, THF ≈ 10^{-20} for heights around 1 km). To avoid possible numerical problems in the analysis associated with small numbers, we scaled each THF with its maximum

value before the analysis and undid this scaling at coefficient level. The dimensionless degree variances of the THFs

$$\sigma H_n^{(p)2} = \sum_{m=1}^{n} \left(\overline{HC}_{nm}^{(p)2} + \overline{HS}_{nm}^{(p)2} \right) \tag{18}$$

are shown in Fig. 4 as a function of the degree n for the first four integer powers.

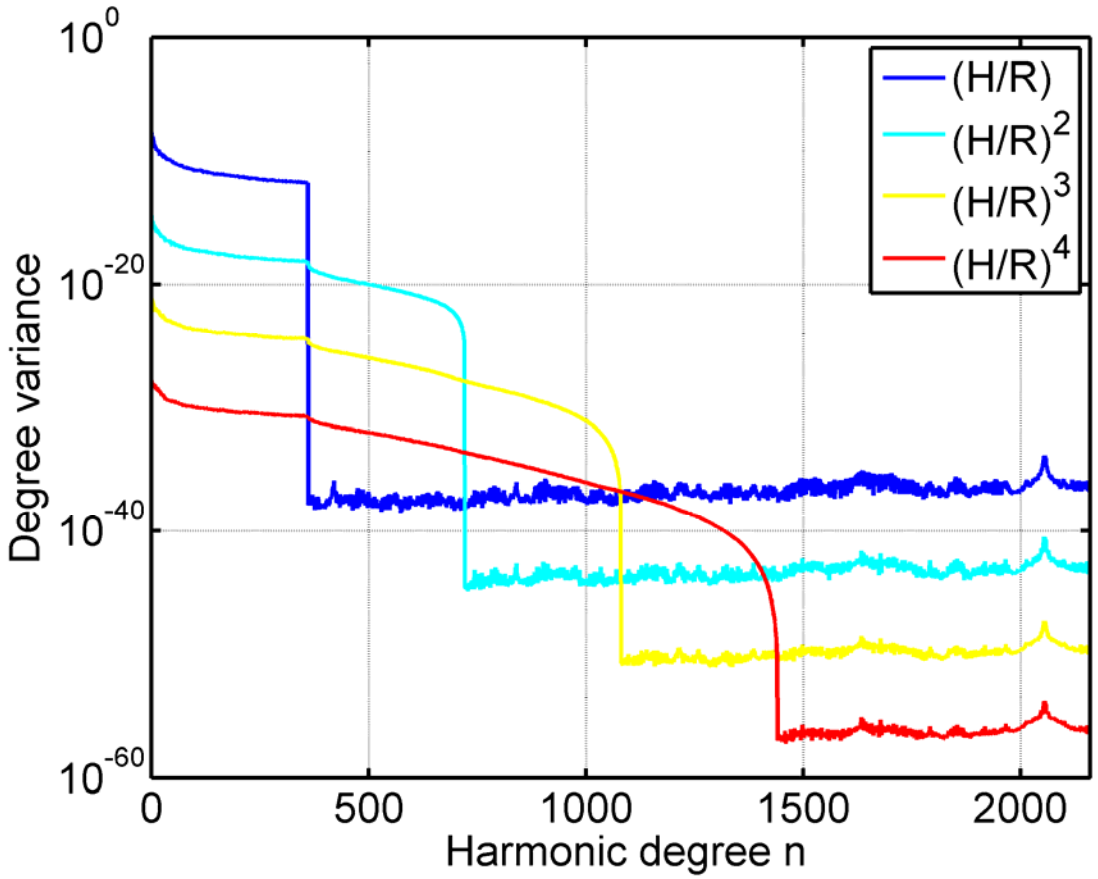

Figure 4. Degree variances of the first four integer powers p of the topographic height function (H/R) band-limited to degree 360

For the linear THF $H^{(1)}$, the spectrum slowly decays from degree 0 to degree 360, drops by 25 orders of magnitude at degree 361, and stays at the level of $\sim 10^{-37}$ for all other degrees (noise level as given by the computational precision). This behaviour is expected, given the band-width limitation of the input topography to $n_{\max} = 360$. The squared THF $H^{(2)}$ is smaller in amplitude, so features less power than $H^{(1)}$. The spectrum of $H^{(2)}$ slowly decays to degree 360, drops slightly around degree 361, and experiences another slow decay up to degree 720, before falling to noise level. This behaviour shows that the band width of $H^{(2)}$ is extended by factor 2 compared to the input band (through rising to power 2). Fig. 4 further shows for the cubed THF

$H^{(3)}$ significant spectral power in band 0 to 1080 (three times the input band width), and for $H^{(4)}$ significant spectral power to degree 1440 (four times the input band width), Exemplified with the first four integer powers of the THFs, Fig. 4 nicely shows the increase in band width by a factor of p with respect to the input band limitation to $n_{max} = 360$.

3.3.2 Potential

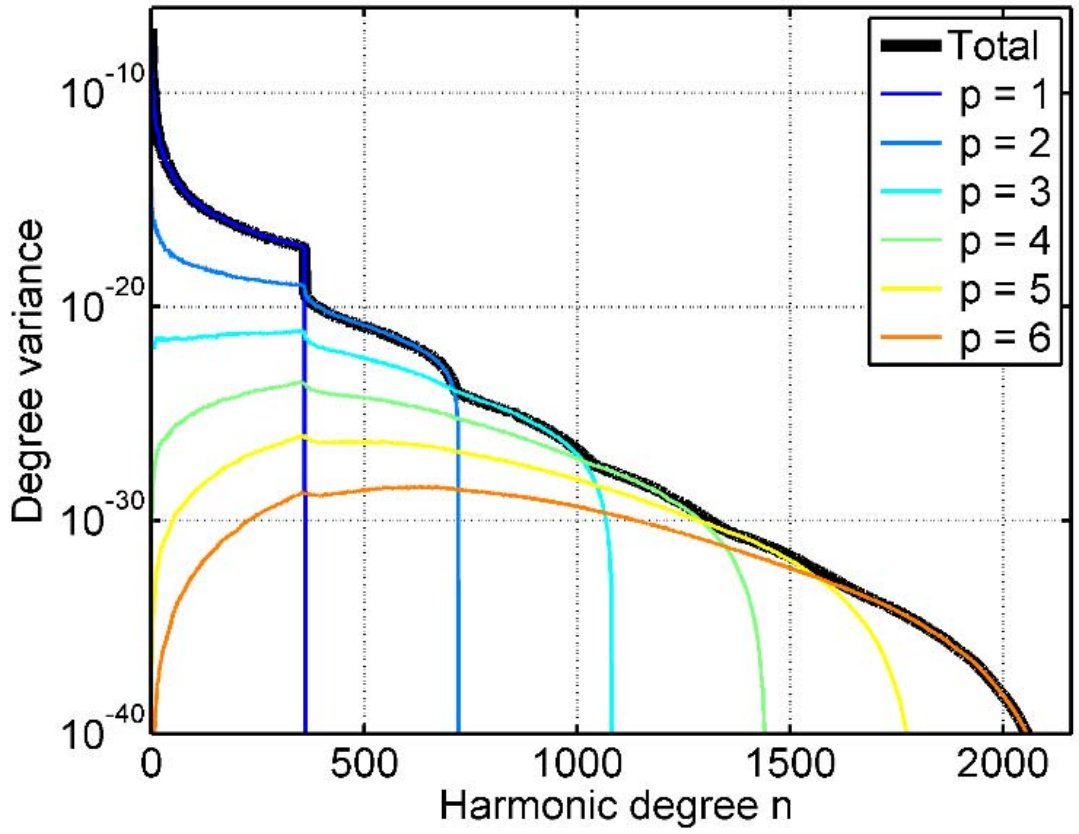

Figure 5. Potential degree variances of the contributions made by the first six integer powers of the topography to the topographic potential (blue to orange), and of potential degree variances of the [resulting] total topographic potential (black line). Topography is band-limited to degree and order 360.

We separately evaluated Eq. (12) for powers $p = 1$ to 6, giving us the p-th contribution of the topography to the topographic potential $V_{nm}^{(p)}$. The dimensionless potential degree variances

$$\sigma V_n^{(p)2} = \sum_{m=1}^{n} \left(\overline{VC}_{nm}^{(p)2} + \overline{VS}_{nm}^{(p)2} \right) \qquad (19)$$

are shown in Fig. 5, as well as the degree variances of the total topographic potential $V_{nm}^{p\max=6}$ (sum of the six contributions $V_{nm}^{(p)}$). As expected from Fig. 4, the contribution made by $p = 1$ only possesses power to $n_{\max} = 360$, while the other five integer powers contribute to degree 720 ($p = 2$), to 1080 ($p = 3$), all the way to degree ~2160 ($p = 6$). Assuming that degree variances below the level of about $\sim 10^{-27}$ are negligible [see *Hirt and Kuhn,* 2012], Fig. 5 suggests that the powers $p = 2$ to 5 contribute significantly to $V_{nm}^{p\max=6}$ in band $[361 \quad 720]$, and powers $p = 3$ to 4 in band [721 1080]. The higher-order contributions of a band-limited topography to the topographic potential tend to contribute largest well beyond the initial input band width, as is seen from the degree variances for $p = 6$, which are maximum near degree ~700, though originating from a topography band limited to $n_{\max} = 360$.

3.4 Spatial analyses

This section compares gravity disturbances from spatial forward modelling (Sect. 2.1) and from spectral forward modelling (Sect. 2.2) over the Himalaya test region ($25° < \varphi < 35°$ and $85° < \lambda < 95°$). Because of the most rugged topography and thus gravitational field, this area should serve as a 'worst-case' test area for the technique comparison. Common to the application of both techniques is the dense computation point spacing of 1 arc-min, as well as the arrangement of computation points at the surface of the topography H. This takes into account attenuation of gravity with height. Over areas where $H < 0$, the computation is carried out at $H = 0$ (avoiding computations inside the reference sphere).

In the spatial domain forward modelling, topographic mass effects induced by the global topography were analytically computed using the discretised Newtonian integration approach described in Sect 2.1. Heights from the topography model were synthesized over the test area in terms of densely spaced grids (20 arc-sec resolution) in spectral band $[0 \quad n_{\max} = 360]$. As such, the grid of topographic heights is highly oversampled by a factor of 90 (note that the maximum harmonic degree of 360 corresponds to a formal spatial resolution of 1800 arc-sec or ~50 km at the equator). In other words, the spherical harmonic topography is very well represented in the space domain through dense grid point spacing. This oversampling minimizes discretisation errors in spatial domain forward modelling.

To reduce computation times, a number of grid resolutions were used as follows: 20-arc-sec within 1° radius, 1 arc-min within 3° radius and 3 arc-min beyond. Because of the quadratic attenuation of gravity with distance, the use of lower grid resolutions outside some radius is common practice (e.g., *Forsberg* [1984]) and – if selected properly – results in approximation errors well below one μGal. Figure 6 shows the gravity disturbances from input band $[0 \quad n_{\max} = 360]$ over our test area, as obtained from the spatial forward modelling (Newtonian integration).

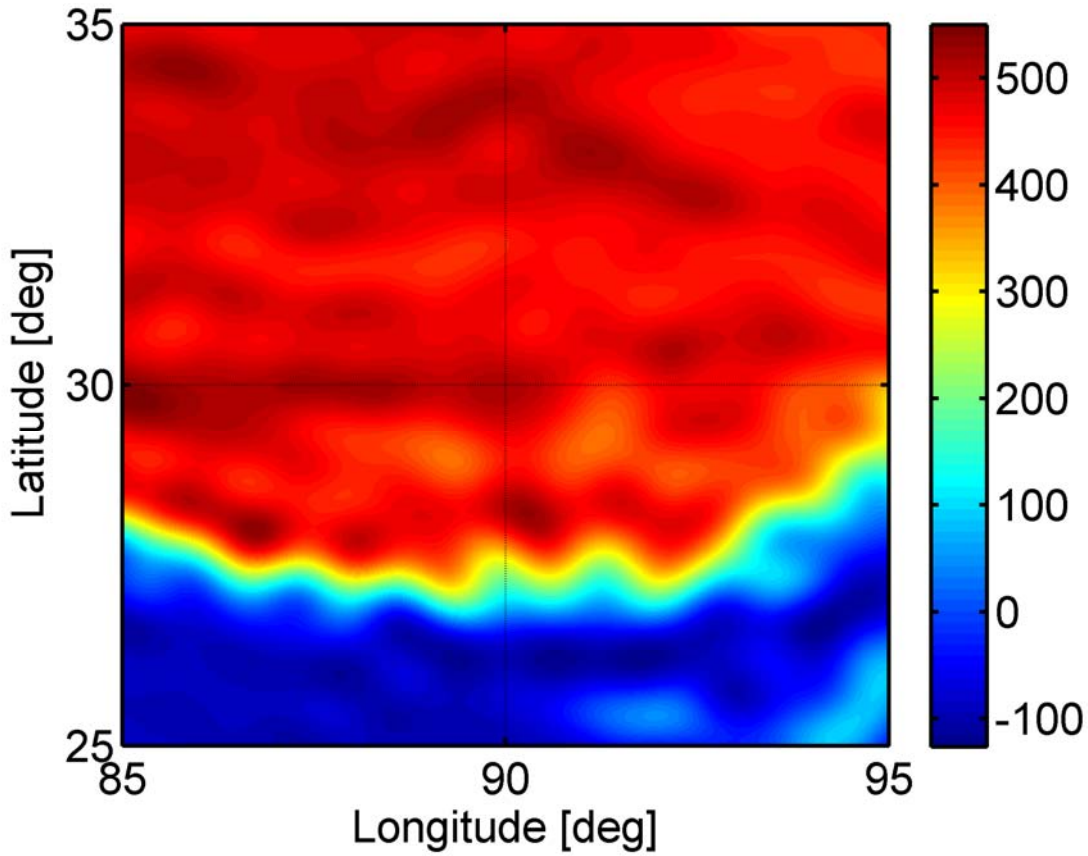

Figure 6. Topographic gravity over the Himalaya test area from space-domain gravity forward-modelling (Newton integration), topographic input band width limited to degree and order 360, unit in mGal (= 10^{-5} m s^{-2}).

Following the contribution scheme of spectral forward modelling, we computed gravity disturbances as a function of (i) the integer power p, and of (ii) the band width

$$[0 \quad n_{\max}], \qquad p = 1$$

$$[(p-1)n_{\max} + 1 \quad pn_{\max}], \qquad p > 1,$$

respectively. The calculation of each individual contribution made by the topography to the topography-implied gravity disturbance is based on continuation with higher-order gravity gradients to $k_{\max} = 10$ and an average reference height $H_{ref} = 3000$ m [Eqs. (15), (16)]. From a comparison with gravity from direct 3D spherical harmonic synthesis (Eq. 13) at the surface of the topography, approximation errors were below 0.1 μGal (tested for $p_{\max} = 6$ and $N_{\max} = 1440$), so safely negligible.

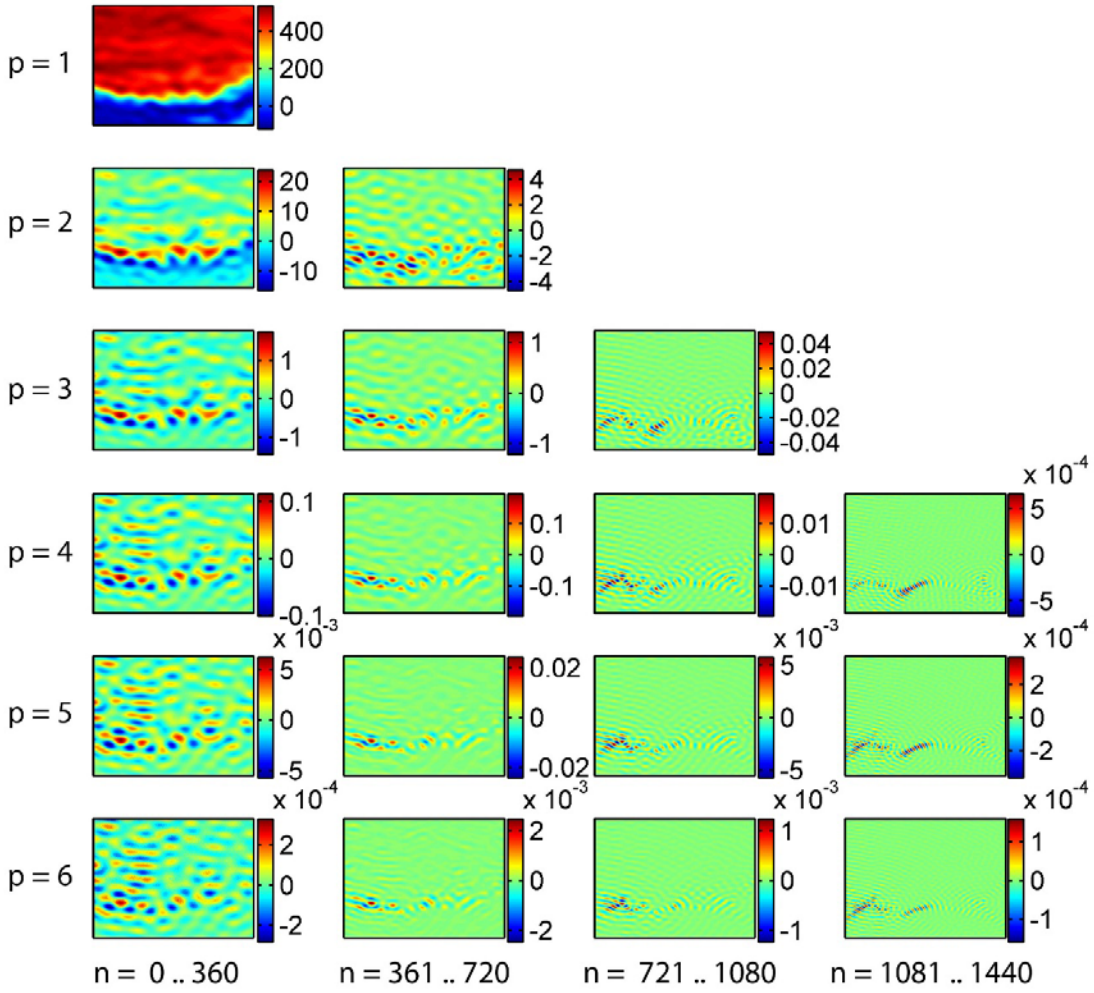

Figure 7. Single contributions of the topography to the topographic gravity over the Himalaya area ($25°<\varphi<35°$, $85°<\lambda<95°$) as a function of the integer power p (increasing from top to bottom), and of the p-th multiple of the input band (increasing from left to right). Input band is limited to harmonic degree 360, unit in mGal.

The spectral contributions of the topography to the gravity disturbance are displayed in Fig. 7 over our test area, whereby the arrangement of panels follows the scheme introduced in Fig. 2. The bulk of the gravity signal originates from the linear term ($p=1$) evaluated to $n_{max}=360$ (top left). It is seen that from $p=1$ to 4 the contributions gradually decrease to the 0.1 mGal level and diminish for higher-order powers. The three columns to the right show the topography-implied signals in bands [361 720], [721 1080] and [1081 1440]. These are all multiples of the input band width which were not considered in previous 'traditional' spectral domain forward modelling. From Fig. 7, the squared and cubed topography generates gravity signals larger than 1 mGal, both within and beyond the input band limitation $n_{max}=360$. Contributions larger than 10 μGal are made by $p=1$ to 5 in band [361 720], and $p=3$ to 4 in band [721 1080], while the contributions associated with band [1081 1440] are below the 1 μGal-level. Qualitatively, this is in good agreement with the spectral analyses made in Sect. 3.3.2.

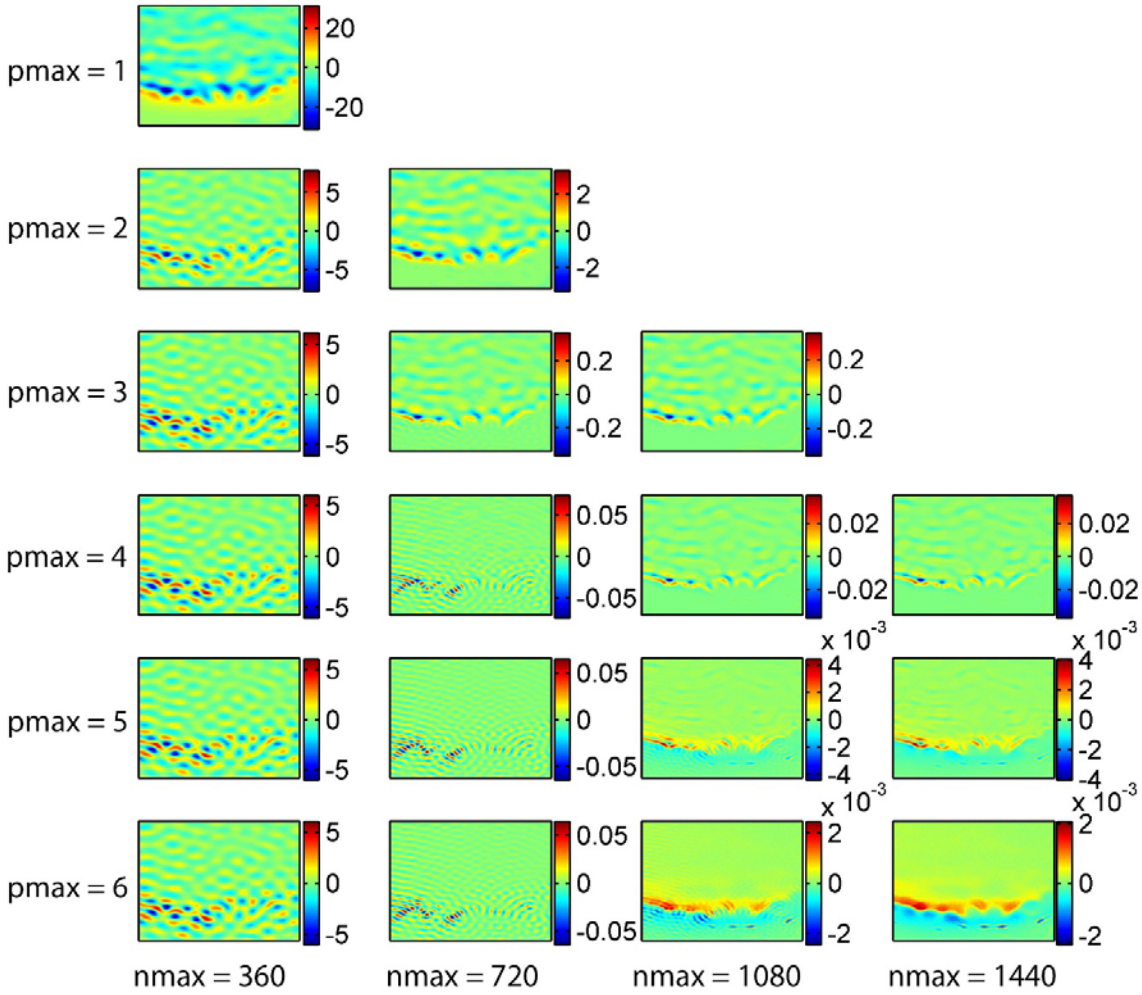

Figure 8. Residuals between topographic gravity from spatial and spectral forward modelling as a function of (i) maximum integer power $p_{\max}$ (increasing from top to bottom) and (ii) maximum harmonic degree $N_{\max}$ (increasing from left to right) used in the spectral-domain forward-modelling. Figure should be read together with Figure 7. Differences are in the sense spectral minus spatial modelling, units in mGal.

As the central result of this study, Fig. 8 shows the differences between gravity disturbances from spectral domain and spatial domain forward modelling as a function of the maximum integer power $p_{\max}$ used in Eq. (12), and the maximum harmonic degree $N_{\max} = pn_{\max}$ evaluated in the spectral domain. The arrangement of panels follows Fig. 7, but the spectral contributions are accumulated, i.e., sums computed to $p_{\max}$ and $N_{\max}$. Selected descriptive statistics (root mean square, and maximum absolute value of the difference) are reported in Table 1. From Fig. 7 and Table 1, the agreement among the two techniques improves with increasing $p_{\max}$ and increasing $N_{\max}$, from ~5 mGal RMS (31 mGal maximum difference) for $p_{\max}$ = 1 and $N_{\max} = n_{\max}$ =360 to an excellent level of 0.3 μGal RMS (~2 μGal maximum difference) for $p_{\max}$ =6 and $N_{\max} \geq$ 1080, see Table 1.

529 **Table 1.** Residuals between spectral and spatial domain forward modelling. Reported are the root-mean square, and
530 in brackets the maximum absolute difference between gravity from the two techniques, unit in mGal.

	Nmax = 360	Nmax = 720	Nmax = 1080	Nmax = 1440
pmax = 1	5.43(31.34)	n/a	n/a	n/a
pmax = 2	1.03(7.83)	0.38 (3.30)	n/a	n/a
pmax = 3	0.96(6.17)	0.03 (0.37)	0.03 (0.36)	n/a
pmax = 4	0.96(6.06)	7.6×10^{-3} (7.5×10^{-2})	2.5×10^{-3} (3.8×10^{-2})	2.5×10^{-3} (3.8×10^{-2})
pmax = 5	0.96(6.06)	7.3×10^{-3} (6.5×10^{-2})	4×10^{-4} (4.4×10^{-3})	4×10^{-4} (4.1×10^{-3})
pmax = 6	0.96(6.06)	7.3×10^{-3} (6.4×10^{-2})	4×10^{-4} (2.5×10^{-3})	3×10^{-4} (2.1×10^{-3})

531

532 Focussing on the left column ($N_{\max}=n_{\max}$=360), in Fig. 8, the discrepancies among the two
533 techniques always exceed 5 mGal, irrespective of the $p_{\max}$ chosen. The residuals in the left
534 column thus correspond to a 'traditional' comparison between spectral and spatial forward
535 modelling with spectral consistency among topography and gravity presumed. Most importantly,
536 it is the consideration of multiples of the input band width that improves the agreement by a
537 factor of ~100 to the 50 μGal level ($N_{\max}=2n_{\max}$=720), and by another factor of ~25 to the μGal
538 level ($N_{\max}=3n_{\max}$=1080), also see Table 1.

539 The comparisons demonstrate that the Newtonian integration inherently 'captures' the additional
540 high-frequency signals (beyond $n_{\max}$), without explicit modelling as must be done in the spectral
541 domain. The remaining discrepancies are likely to reflect numerical integration errors in the
542 spatial domain technique. Further, the comparisons also show (implicitly) sufficient convergence
543 of the series expansions applied for field continuation [Eqs. (15), (16)].

544 **3.5 Computational costs**

545 Regarding the computational costs for spectral domain forward modelling, a spherical harmonic
546 analysis of a single power of the THF took ~3 min on a standard office PC (input topography
547 band limited to degree 360, output coefficients of the THF to degree 2160). With the first six
548 powers of the THF taken into account (Fig. 5), the overall computation time for application of
549 the contribution scheme (Fig. 2) and synthesis of gravity effects with gradients over our 10°x10°
550 study area (360,000 points) was less than 1 hour. Opposed to this, the Newton integration
551 required more than 10,000 CPU hours on Western Australia's iVec supercomputer to provide
552 gravity effects over the same area. The computational costs of the space domain technique were
553 relatively high because of the oversampling (20 arc-sec grid resolution for a degree-360 signal)
554 that was chosen to reduce discretisation errors down to the microGal-level. Polyhedral bodies
555 instead of prisms may not require such extreme oversampling to yield similarly low
556 discretisation errors, thus reducing the computational cost.

While in the case study the spectral technique was numerically more efficient than the spatial technique, there is a clear tendency of the spectral method becoming much more computationally intensive as the degree increases. Application of the contribution scheme in Fig. 2 for a source topography model to degree-2160 (10 km resolution) would require multiple harmonic synthesis e.g., to degree and order 10,800 (five times oversampling) to "capture" the short-scale gravity signals at spatial scales less than 10 km. Currently, there is no software at hand to accurately gauge the computational costs for this or other high-degree applications of the contribution scheme. Importantly, increasing the spectral resolution will increase the computation times for spectral forward modelling but not for the Newton integration if the above grid resolutions remain the same.

4. Discussion

Gravity disturbances obtained from two entirely independent modelling techniques, but from the same input mass distribution, were compared over a worst-case test area, with special focus on the spectral domain contributions made by (i) the integer powers p of the topography, and (ii) multiples p of the input band width. Our numerical tests unambiguously demonstrate that a band-limited topographic mass distribution implies a gravitational field with spectral power far beyond the input band limitation to $n_{\max}$. Our test procedures were sensitive enough to empirically show the relevance of the first three multiples ($N_{\max} = 4\,n_{\max}$) of the input band, as well as of higher-order contributions up to $p = 6$. This provides strong evidence for the validity of the contribution scheme introduced in Fig. 2, and thus justifies the statement that a band-limited topography generates (in good approximation) a full-spectrum gravity field.

The discrepancies among gravity from the spectral and spatial techniques were found to be smaller than ~2 μGal when integer power contributions to $p_{\max} = 6$ were evaluated, and the band width of the potential was extended by a factor 4 over the band width of the topography ($N_{\max} = 4\,n_{\max}$). With a maximum signal strength of ~500 mGal (Fig. 6), this translates into a relative error of 4×10^{-6}. To our knowledge, such a low relative error among the two forward modelling techniques has not yet been reported in the literature. Compared to the uncertainty of the universal gravitational constant G of about 1.2×10^{-4} [*Mohr et al.,* 2012, p 72], these technique discrepancies play a diminishing role for the accurate computation of topography-generated gravity. All in all, the level of agreement between the forward modelling techniques can be considered as excellent.

Holistically, our numerical comparisons provide valuable mutual feedback on the two techniques applied, contributing to a better understanding of gravity forward modelling. In particular, the comparisons demonstrate the following:

- The importance of the computation point height. For the meaningful calculation of gravity disturbances (or other functionals of the potential), computation points in both techniques were located at the topography (other locations are possible). While the attenuation of gravity with height and distance from the generating masses is accounted for through the choice of computation points in the Newtonian integration, consideration is possible in the spectral domain through gravity synthesis at the surface of the topography. The excellent agreement between gravity from the two techniques (Table 1) implicitly shows convergence of the gradient solution applied here [Eqs. (16), (17)].

- The importance of higher-order integer contributions. For the accurate application of spectral domain forward modelling higher-order contributions made by integer powers of the topography become increasingly relevant as the resolution of the input topography increases [see also *Hirt and Kuhn*, 2012]. While the theory [e.g., *Rummel et al.,* 1988; *Wieczorek and Phillips*, 1998] clearly shows the need for higher-order contributions, there are only few studies concerned with empirical verification of these terms based on independent or external methods. *Chambat and Valette* [2005] showed the relevance of the squared topographic contribution (via a comparison with geopotential models). Our technique comparisons now demonstrate the relevance of integer powers up to the sixth power.

- The importance of multiples of the input band width. To accurately compute the gravitational field implied by a topographic mass distribution in the spectral domain, the contributions of the higher-order powers must be calculated in multiples of the input band width. The additional high-frequency gravity signals are significant (in our tests up to four times the input band width), as was shown by comparison with the independent Newtonian integration.

When the additional high-frequency signals remained [deliberately] unmodelled in our study (i.e., $N_{\max} = n_{\max}$), the discrepancies among the two techniques would translate into relative errors of ~1% ($N_{\max} = n_{\max}$ = 360, cf. Table 1), but this will be larger for $N_{\max} = n_{\max} > 360$. Not shown here for the sake of brevity, but a second numerical test with input band $N_{\max} = n_{\max}$ = 2160 yielded ~6.5% relative errors (34 mGal maximum discrepancy among both techniques vs. ~530 mGal signal) when neglecting signals beyond the input band width in the spectral technique. These magnitudes are comparable with relative errors encountered in other studies comparing spectral and spatial forward modelling (0.8%, *Novak and Tenzer* [2013]; 3%, *Kuhn and Seitz* [2005]; 4.5 %, *Wild-Pfeiffer and Heck* [2007], and ~10%, *Wang et al.* [2010]; *Balmino et al.* [2012], please see Sect. 1). Given our relative errors are at the level of 10^{-4} (0.01 %) for $N_{\max} = 2n_{\max}$ = 720, and diminish to the level of 4×10^{-6} (0.0004%) for $N_{\max} = 4n_{\max}$ =1440, it is

629 safe to conclude that [unmodelled und usually truncated] topography-generated gravity signals
630 beyond n_{max} are a key candidate for the discrepancies among spectral and spatial forward
631 modelling encountered in the aforementioned studies.

632 *Wieczorek* [2007] noted in his review paper on the character of the spectral forward modelling
633 equation [Eq. (12) in this paper]: "*While the sum of Eq. 30 [ibid, p 19] is finite, and hence exact,*
634 *the number of terms grows linearly with spherical harmonic degree*". However, our results and
635 the contribution scheme (Fig. 2) show that the sum used by *Wieczorek* [2007] cannot be used for
636 the exact computation of gravity implied by a given topography, because spectral consistency
637 among gravity and topography is assumed when using $N_{max} = n_{max}$. Rather, the *exact* calculation
638 of gravity from topography by harmonic expansion requires consideration of $N_{max} = p_{max} n_{max}$
639 [Eq. (10)], as shown in this study.

640 **5. Conclusions**

641 This paper has investigated the spectral (band width) inconsistency among spherical harmonic
642 topographic mass models and the generated gravitational field. A generalized contribution
643 scheme was introduced for the spectral domain forward modelling technique as a function of
644 integer powers and multiples of the input topography's band width. This new scheme
645 mathematically describes the extension of the spectrum associated with the transformation of
646 topography to gravity based on Newton's law of gravitation. The short-scale gravity signals
647 generated by a band-limited topography can be surprisingly easily modelled in the spectral
648 domain as shown in this paper. The validity of the contribution scheme was confirmed through
649 spectral analyses and space domain comparisons.

650 Modelling the additional high-frequency signals beyond the input band width has brought
651 together the spatial domain and spectral domain forward modelling technique from a level of 10^{-2}
652 to the level of better than 10^{-5} in terms of gravity disturbances. This is a considerable
653 improvement by three orders of magnitude.

654 There are applications where the spectral inconsistency between topographic mass models and
655 gravitational potential is entirely uncritical. For instance comparisons between observed and
656 topography-implied gravitational fields in spherical harmonics (as in the calculation of spherical
657 harmonic Bouguer gravity). This is because the fields are spectrally consistent in the gravity
658 domain.

659 However, if the gravitational field generated by a spherical harmonic topography is to be exactly
660 calculated, then multiples of the input topography's band width should be computed and
661 evaluated in the spectral domain. Multiples of the input band width can be expected to become
662 more relevant as the resolution increases (cf. Sect. 4). This has important implications for present
663 and future ultra-high degree models of the topographic potential: For a standard degree-2160
664 topography model, the implied topographic potential would have to be modelled to (a coarsely

665 estimated) degree of ~10,800 or higher if sufficient consistency between the two quantities is
666 sought. For an input band width of a topography model to degree and order 10,800 [e.g.,
667 *Balmino et al.,* 2012] would require spectral domain modelling to extremely high degree to
668 accurately compute the generated gravitational potential.

669 Finally, with the understanding of the spectral domain technique drawn from this study,
670 comparisons among spectral domain and spatial domain forward modelling can now be much
671 better utilized for a mutual validation of forward modelling software implementations and
672 detailed testing of forward-modelling approaches. For instance, this can be helpful for (i) testing
673 integration formulas for gravity effects from mass bodies [*Grombein et al.,* 2013, *d'Urso* 2014]
674 in the spatial domain technique, or (ii) investigating the convergence behaviour of series
675 expansions in the spectral domain in some not entirely undisputed cases (e.g., evaluations inside
676 the masses or inside the reference body).

677 **Acknowledgement**

678 We thank the Australian Research Council (ARC) for funding through discovery project grant
679 DP120102441. This study was partially supported by Technische Universität München (TUM) –
680 Institute for Advanced Study (IAS), funded by the German Excellence Initiative and the
681 European Union Seventh Framework Programme under grant agreement n° 291763. Christian
682 Hirt is the recipient of an ARC DORA award and a TUM/IAS Hans-Fischer Fellowship. Mark
683 Wieczorek is thanked for advice on his SHTools software package, and Sten Claessens for the
684 hint on the GRS80 reference field being an analogy to our work. We thank two reviewers for
685 their valuable comments on our manuscript, and the editor for the manuscript handling. Western
686 Austalia's ivec supercomputing facility (www.ivec.org) was used for parts of the calculations
687 presented in this work.
688

689 **Literature**

690 Anderson, E.G. (1976),The effect of topography on solutions of Stokes' problem. Unisurv S-14 Report,
691 *School of Surveying*, University of New South Wales, Kensington.
692 Bagherbandi M., and L.E. Sjöberg (2012), A synthetic Earth gravity model based on a topographic-
693 isostatic model, *Stud. Geophys. Geod.,* 56(2012), 935-955, doi: 10.1007/s11200-011-9045-1.
694 Balmino, G., N. Vales, S. Bonvalot and A. Briais (2012), Spherical harmonic modelling to ultra-high
695 degree of Bouguer and isostatic anomalies, *J. Geod.,* 86(7), 499-520, doi: 10.1007/s00190-011-
696 0533-4.
697 Benedek J. (2004), The application of polyhedron volume elements in the calculation of gravity related
698 quantities, *Special Issue of Österreichische Beiträge zu Meteorologie und Geophysik*, 31, 99-106.
699 Brigham, E.O. (1988), *The Fast Fourier Transform and Its Applications*, Prentice Hall, New Jersey, 448p
700 Bucha, B. and Janák, J. (2013), A MATLAB-based graphical user interface program for computing
701 functionals of the geopotential up to ultra-high degrees and orders, *Computers and Geosciences*,
702 56, 186-196, doi: 10.1016/j.cageo.2013.03.012.

Chambat, F., and B. Valette (2005), Earth gravity up to second order in topography and density, *Physics Earth Plan. Int,* 151 (1-2) 89-106, doi:10.1016/j.pepi.2005.01.002.

Claessens S.J. and C. Hirt (2013), Ellipsoidal topographic potential - new solutions for spectral forward gravity modelling of topography with respect to a reference ellipsoid, *J. Geophys. Res.,*118(11), 5991-6002, doi: 10.1002/2013JB010457.

Driscoll J.R., and D.M. Healy (1994), Computing Fourier transforms and convolutions on the 2-sphere, *Adv. in Appl. Math.*, 15, 202-250.

D'Urso, M. G. (2014), Analytical computation of gravity effects for polyhedral bodies*, J. Geod.,* 88(1), 13-29, doi:10.1007/s00190-013-0664-x

Eshagh, M. (2009), Comparison of two approaches for considering laterally varying density in topographic effect on satellite gravity gradiometric data. *Act. Geoph.,* 58(4), 661-686, doi: 10.2478/s11600-009-0057-y.

Forsberg R. (1984), A study of terrain reductions, density anomalies and geophysical inversion methods in gravity field modelling. *Report* 355, Department of Geodetic Science and Surveying, Ohio State University, Columbus.

Fukushima T. (2012a), Numerical computation of spherical harmonics of arbitrary degree and order by extending exponent of floating point numbers. *J. Geod.,* 86(4), 271–285, doi: 10.1007/s00190-011-0519-2.

Fukushima T. (2012b), numerical computation of spherical harmonics of arbitrary degree and order by extending exponent of floating point numbers: II first-, second-, and third-order derivatives, *J Geod.,* 86(11), 1019-1028, doi:10.1007/s00190-012-0561-8.

Grombein T, Seitz K, Heck B (2013), Optimized formulas for the gravitational field of a tesseroid. *J Geod.* 87(7), 645–660. doi:10.1007/s00190-013-0636-1

Gruber C., Novák P., F. Flechtner and F. Barthelmes (2013), Derivation of the topographic potential from global DEM models*, International Association of Geodesy Symposia* 139, Springer-Verlag Berlin Heidelberg, 535-542, doi: 10.1007/978-3-642-37222-3__71.

Grüninger, W. (1990), Zur topographisch-isostatischen Reduktion der Schwere. *PhD Thesis*, Universität Karlsruhe.

Jacoby, W., and P.L. Smilde (2009), *Gravity interpretation,* Springer, Berlin, Heidelberg.

Heck, B., and K. Seitz (1991), Nonlinear Effects in the Scalar Free Geodetic Boundary Value Problem, Spherical Harmonic Representation of the Effects on the Reduced Boundary Condition, the Disturbing Potential and the Vertical Position Correction, Report, 78 pages, Institute of Geodesy, University of Stuttgart, ISSN 0933-2839.

Heck, B., and K. Seitz (2007), A comparison of the tesseroid, prism and point-mass approaches for mass reductions in gravity field modelling. *J Geod.,* 81(2), 121-136, doi: 10.1007/s00190-006-0094-0.

Hirt, C., U. Marti, B. Bürki, and W.E. Featherstone (2010), Assessment of EGM2008 in Europe using accurate astrogeodetic vertical deflections and omission error estimates from SRTM/DTM2006.0 residual terrain model data, *J. Geophys. Res.,* 115, B10404, doi: 10.1029/2009JB007057.

Hirt, C., M. Kuhn, W.E. Featherstone, and F. Göttl (2012), Topographic/isostatic evaluation of new-generation GOCE gravity field models, *J. Geophys. Res.,* 117, B05407, doi:10.1029/2011JB008878.

Hirt, C., and M. Kuhn (2012), Evaluation of high-degree series expansions of the topographic potential to higher-order powers, *J. Geophys. Res.,* 117, B12407, doi:10.1029/2012JB009492.

Hirt, C. (2012), Efficient and accurate high-degree spherical harmonic synthesis of gravity field functionals at the Earth's surface using the gradient approach, *J. Geod.,* 86(9), 729-744, doi: 10.1007/s00190-012-0550-y.

Hirt, C. (2013), RTM gravity forward-modeling using topography/bathymetry data to improve high-degree global geopotential models in the coastal zone, *Marine Geod.,* 36(2), 1-20, doi:10.1080/01490419.2013.779334.

Holmes S.A., and W.E. Featherstone (2002),A unified approach to the Clenshaw summation and the recursive computation of very high degree and order normalized associated Legendre functions, *J. Geod.,* 76(5), 279-299,doi: 10.1007/s00190-002-0216-2.

Holmes, S. A., and N. K. Pavlis (2008), Spherical harmonic synthesis software harmonic_synth. Available at: http://earth-info.nga.mil/GandG/wgs84/gravitymod/egm2008/index.html.

Kuhn, M. (2000), Geoidbestimmung unter Verwendung verschiedener Dichtehypothesen, Reihe C, Heft Nr. 520. *Deutsche Geodätische Kommission*, München.

Kuhn, M. (2003), Geoid determination with density hypotheses from isostatic models and geological information, *J. Geod.*, 77(1-2), 50-65, doi: 10.1007/s00190-002-0297-y.

Kuhn, M., and W.E. Featherstone. (2003), On the Construction of a Synthetic Earth Gravity Model, In: *Proceed 3rd Meeting of the Intern. Gravity and Geoid Commission*, ed. I Tziavos, 189-194. Editions Ziti.

Kuhn, M., and K. Seitz (2005), Comparison of Newton's Integral in the Space and Frequency Domains, in *A Window on the Future of Geodesy*, IAG Symposia vol. 128, ed F Sanso, 386-391.

Kuhn, M., W.E. Featherstone, and J.F. Kirby (2009), Complete spherical Bouguer gravity anomalies over Australia, *Australian J. Earth Sci.,* 56, 213-223.

Mader, K. (1951), Das Newtonsche Raumpotential prismatischer Körper und seine Ableitungen bis zur dritten Ordnung. *Österreichische Zeitschrift für Vermessungswesen*, Sonderheft 11.

Makhloof, A.A. (2007), The Use of Topographic-Isostatic Mass Information in Geodetic Applications, *Dissertation*, Institut für Geodäsie und Geoinformation der Universität Bonn, D 98.

Moritz, H. (2000), Geodetic Reference System 1980, *J. Geod.,* 74(1), 128-162, doi: 10.1007/s001900050278.

Mohr P.J., B.N. Taylor, and D.B. Newell (2012), "The 2010 CODATA Recommended Values of the Fundamental Physical Constants" (Dated: March 25, 2012). Available from http://physics.nist.gov/constants.

Nagy, D. (1966), The gravitational attraction of a right rectangular prism. *Geophysics*, 31, 362-371.

Nagy, D., G. Papp, and J. Benedek (2000), The gravitational potential and its derivatives for the prism. *J. Geod.* 74(7), 552-560, Erratum in *J. Geod.,* 76(8):475.

Novák, P. (2010), Direct modelling of the gravitational field using harmonic series, *Acta Geodyn. Geomater.*, 7(1), 35-47.

Novák, P. and R. Tenzer (2013), Gravitational Gradients at Satellite Altitudes in Global Geophysical Studies, *Surv. Geophys.* 34, 653-673, doi: 10.107/s10712-013-9243-1.

Pavlis N.K., and R.H. Rapp (1990), The development of an isostatic gravitational model to degree 360 and its use in global gravity modelling. *Geophys. J. Int.,* 100, 369-378.

Papp G. and Z.T. Wang (1996), Truncation effects in using spherical harmonic expansions for forward local gravity field modelling. *Acta Geod. Geophys. Hung.* 31(1-2), 47-66.

Rapp, R.H. (1989), The decay of the spectrum of the gravitational potential and the topography of the Earth, *Geophys. J. Int.,* 99, 449-455.

790 Rapp, R.H., and N.K. Pavlis (1990), The development and analysis of geopotential coefficient models to
791 spherical harmonic degree 360, *J. Geophys. Res.,* 95(B13), 21885-21911.
792 Rummel, R., R.H. Rapp, H. Sünkel, and C.C. Tscherning (1988), Comparisons of global
793 topographic/isostatic models to the Earth's observed gravity field, *Report* No 388, Dep. Geodetic
794 Sci. Surv., Ohio State University, Columbus, Ohio.
795 Sünkel, H. (1985), An isostatic Earth model, *Report* No 367, Dep. Geodetic Sci. Surv., Ohio State
796 University, Columbus, Ohio.
797 Tenzer, R. (2005), Spectral domain of Newton's integral, *Boll Geod. Sci. Affini*, 2, 61-73
798 Tenzer, R., P. Novák, P. Vajda, V. Gladkikh, and Hamayun (2012), Spectral harmonic analysis and
799 synthesis of Earth's crust gravity field, *Comput. Geosci.,*16, 193-207, doi:10.1007/s10596-011-
800 9264-0
801 Tsoulis, D. (2001), A comparison between the Airy/Heiskanen and the Pratt/Hayfordisostatic models for
802 the computation of potential harmonic coefficients, *J. Geod.,* 74(9), 637-643,
803 doi:10.1007/s001900000124.
804 Tsoulis, D., P. Novák, and M. Kadlec (2009), Evaluation of precise terrain effects using high-resolution
805 digital elevation, models, *J. Geophys. Res.,* 114, B02404, doi:10.1029/2008JB005639.
806 Tziavos, I.N., and M.G. Sideris (2013), Topographic Reductions in Gravity and Geoid Modeling. *Lecture*
807 *Notes in Earth System Sciences* 110, 337-400, Springer, Berlin Heidelberg.
808 Wang, Y.M., S. Holmes, J. Saleh, X.P. Li and D. Roman (2010), A comparison of topographic effect by
809 Newton's integral and high degree spherical harmonic expansion – Preliminary Results, poster
810 presented at *WPGM 2010 Taipei*, Taiwan, June 22 -25.
811 Wang, Y.M., and X. Yang (2013) On the spherical and spheroidal harmonic expansion of the
812 gravitational potential of topographic masses, *J. Geod.*, 87(10-12), 909-921, doi:10.1007/s00190-
813 013-0654-z.
814 Wieczorek, M.A. (2007), Gravity and topography of the terrestrial planets. In *Treatise on Geophysics,* 10,
815 165-206, Elsevier-Pergamon, Oxford, United Kingdom.
816 Wieczorek, M.A., and R.J. Phillips (1998), Potential anomalies on the sphere: Applications to the
817 thickness of the lunar crust, *J. Geophys. Res.,* 103(E1), 1715-1724, doi:10.1029/97JE03136.
818 Wild-Pfeiffer F., and B. Heck (2007), Comparison of the modelling of topographic and isostatic masses in
819 the space and the frequency domain for use in satellite gravity gradiometry, in *Gravity Field of the*
820 *Earth*, Proceed. 1st International Symposium of the International Gravity Field Service, Istanbul,
821 Turkey, Harita Dergisi, 312-317.